PAPER • OPEN ACCESS

Hyperfine interactions and coherent spin dynamics of isotopically purified $^{167}{\rm Er}^{3+}$ in polycrystalline ${\rm Y_2O_3}$

To cite this article: Tijana Rajh et al 2022 Mater. Quantum. Technol. 2 045002

View the article online for updates and enhancements.

You may also like

- Matrix isolation in laboratory astrochemistry: state-of-the-art, implications and perspective Vladimir I. Feldman, Sergey V. Ryazantsev and Svetlana V. Kameneva
- Organoelement chemistry: promising growth areas and challenges
 Gleb A. Abakumov, Alexandr V. Piskunov, Vladimir K. Cherkasov et al.
- Current state of the spin exchange theory in dilute solutions of paramagnetic particles. New paradigm of spin exchange and its manifestations in EPR spectroscopy K M Salikhov

Materials for **Quantum Technology**



OPEN ACCESS

RECEIVED

5 August 2022

REVISED

11 October 2022

ACCEPTED FOR PUBLICATION 28 October 2022

PUBLISHED

15 November 2022

Original content from this work may be used under the terms of the Creative Commons Attribution 4.0 licence.

Any further distribution of this work must maintain attribution to the author(s) and the title of the work, journal citation and DOI.



PAPER

Hyperfine interactions and coherent spin dynamics of isotopically purified $^{167}\text{Er}^{3+}$ in polycrystalline Y_2O_3

Tijana Rajh^{1,2,*}, Lei Sun¹, Shobhit Gupta³, Jun Yang⁴, Haitao Zhang⁴ and Tian Zhong^{5,*}

- Center for Nanoscale Materials, Argonne National Laboratory, Argonne, IL 60439, United States of America
- School of Molecular Sciences, Arizona State University, AZ 85287, United States of America
- ³ Department of Physics, University of Chicago, Chicago, IL 60637, United States of America
- Corning Research & Development Corporation, Sullivan Park, Painted Post, NY 14870, United States of America
- Pritzker School of Molecular Engineering, University of Chicago, Chicago, IL 60637, United States of America
- * Authors to whom any correspondence should be addressed.

E-mail: Tijana.Rajh@asu.edu and tzh@uchicago.edu

Keywords: rare-earth ion, electron spin resonance, hyperfine interactions

Supplementary material for this article is available online

Abstract

 $^{167}{\rm Er}^{3+}$ doped solids are a promising platform for quantum technology due to erbium's telecom C-band optical transition and its long hyperfine coherence times. We experimentally study the spin Hamiltonian and dynamics of $^{167}{\rm Er}^{3+}$ spins in $\rm Y_2O_3$ using electron paramagnetic resonance (EPR) spectroscopy. The anisotropic electron Zeeman, hyperfine and nuclear quadrupole matrices are fitted using data obtained by X-band (9.5 GHz) EPR spectroscopy. We perform pulsed EPR spectroscopy to measure spin relaxation time T_1 and coherence time T_2 for the 3 principal axes of an anisotropic g tensor. Long electronic spin coherence time up to 24.4 μ s is measured for lowest g transition at 4 K, exceeding previously reported values at much lower temperatures. Measurements of decoherence mechanism indicates T_2 limited by spectral diffusion and instantaneous diffusion. Long spin coherence times, along with a strong anisotropic hyperfine interaction makes T_2 limited by spectral diffusion and instantaneous diffusion.

1. Introduction

Rare-earth (RE) ions in solids possess shielded 4f intra-shell optical and spin transitions with narrow linewidths and long coherence times [1-3], making them ideal candidates for applications such as quantum memory [1, 4] in a quantum network [5], microwave-to-optical quantum transduction [6] and quantum sensing [7]. Among RE ions, erbium (Er³⁺) in particular, constitutes a unique system that simultaneously possesses optical fiber-compatible telecom C-band optical transition (1535 nm), high electron g-factor (14.6 $\mathrm{Er^{3+}}: Y_2 \mathrm{SiO}_5$) [8] with long nuclear spin coherence time of 1.3 s at 1 K ($^{167}\mathrm{Er^{3+}}: Y_2 \mathrm{SiO}_5$) [3]. $^{167}\mathrm{Er^{3+}}$ with nuclear spin I = 7/2 exhibits strong anisotropic hyperfine interactions, resulting in electron-nuclear hybridized states in low symmetry sites with reduced sensitivity to magnetic field noise at zero field—known as the zerofirst-order Zeeman (ZEFOZ) transitions [9] as well as a large zero field transition frequencies in the microwave range. Narrow optical homogenous and inhomogeneous linewidth [10, 11] have been demonstrated in ¹⁶⁷Er³⁺ doped yttrium orthosilicate (YSO) [3]. Comparable to YSO, yttrium oxide (Y2O3) is another low magnetic noise host with a similar ionic radius of Y³⁺ to Er³⁺ (1.04 vs 1.03 Å) and can be synthesized in diverse range of material platform compatible with nanoscale integration [12] including thin films [13, 14], nanoparticles [15, 16], and transparent polycrystalline ceramics [11]. This combination makes the characterization of spin Hamiltonian of 167 Er3+:Y2O3 crucial to further develop this quantum platform by exploiting its longcoherence-time hyperfine transitions as well as performing coherent control of ¹⁶⁷Er³⁺ spins as a resource for quantum technology applications.

We report X-band (9.5 GHz) electron paramagnetic resonance (EPR) (continuous-wave and pulsed) spectroscopic studies of the atomic environment and dynamics of the Er^{3+} spins in Y_2O_3 polycrystalline matrix.

We investigate the electronic structure of Er^{3+} using continuous-wave (CW) EPR and characterize Er^{3+} local structure variations in different crystalline environments (C_2 and C_{3i}) in cubic Y_2O_3 by determining the Zeeman, hyperfine and quadrupole interactions. We compare X-band EPR with low field C-band (5 GHz) EPR to verify the spin Hamiltonian in a regime where the Zeeman energy is comparable to hyperfine energy. The hyperfine transitions in $^{167}Er^{3+}$ introduce mixed states that show a relatively slow spin relaxation, which can be detected at temperatures of 4.0–6.0 K. We measure a long spin coherence time of 24.4 μ s at 4 K for lowest g-factor transition. The limits for coherence relaxation times given by spin-lattice relaxation (characterized as T_1) is 5 ms at 4.0 K. Our study provides a comprehensive spin spectroscopy of $^{167}Er^{3+}$ in Y_2O_3 , which shows significant prospects of this platform for future applicable quantum technologies.

2. Results and discussion

The ${\rm Er}^{3+}$ ion contains ${\rm 4f}^{11}$ electrons which result in a total spin quantum number of S=3/2, an orbital quantum number of 6 and total angular momentum of J=15/2. The ground level ${}^4I_{15/2}$ is 16-fold degenerate and in the presence of crystal field of low symmetry it can split into 8 (J+1/2) Kramer doublets. The energy of microwave radiation generated in conventional X-band EPR experiments (9.5 GHz) is generally sufficient to probe only the lowest-lying doublet of the ${}^4I_{15/2}$ manifold of trivalent erbium. As a result, common studies of ${\rm Er}^{3+}$ in metal oxides consider only the lowest lying Kramer doublet with an effective spin S=1/2 system to account for the features of ${\rm Er}^{3+}$ EPR spectra:

$$H = \mu_{\rm B} B_0 \cdot \mathbf{g}_e \cdot S_e + S_e \cdot \mathbf{A} \cdot I_{\rm n} + I_{\rm n} \cdot \mathbf{Q} \cdot I_{\rm n}, \tag{1}$$

where the first Zeeman term represents the energy of the electronic spin in a magnetic field B_0 and the second term accounts for the hyperfine interaction with nuclear spins and the third term is nuclear quadrupole interaction, μ_B is the Bohr magneton and g, A and Q are interaction tensors, which reflect local structure particularities of the paramagnetic complex. EPR spectrum of Y_2O_3 doped with natural abundance of Er^{3+} is shown in figure I(a). The sample has a nominal Er^{3+} doping of 20 parts per million (ppm), and was prepared by sintering 40 nm-sized nanocrystals into polycrystalline ceramics according to the method reported in reference [11]. For X-band EPR measurement, the sample was grinded to microparticles to increase the filling factor of the microwave cavity. Figure I(a) inset shows the crystal structure of cubic Y_2O_3 with annotated different local sites available for the substitution of Y^{3+} with Er^{3+} . Two possible sites are: a lower symmetry C_2 site whose substitution should result in a rhombic EPR signal and a higher symmetry trigonal C_{3i} site whose substitution should result in an axial EPR signal. Indeed, we clearly observe four main transitions, three for a rhombic signal ($g_2 = 12.20$, $g_y = 4.89$ and $g_x = 1.64$) and a main signal for trigonal symmetry site ($g_{\perp} = 3.32$). Upon close inspection of the lowest rhombic component using small modulation amplitude, we find that the lowest signal at g = 12.20 is composed of two signals, one with g = 12.20, which is approximately 5 times more intense than the one with g = 12.08 (figure I(b)).

The two signals have different saturation properties suggesting their association with different sites (inset, figure 1(b)). Simulation of the experimental spectra with even isotope $^{166}\text{Er}^{3+}$ (33.5% natural abundance) using the above listed parameters for the parallel component of the axially symmetric signal (C_{3i}) perfectly matched observed transitions and signal's intensity. The average g_{avg} factors for both C_2 and C_{3i} systems were found to be 6.243, suggesting Γ_7 ground state ($g_{ave} = 6.0$) rather than Γ_6 ($g_{ave} = 6.8$) usually found in Er³⁺ doped samples [17–19].

The g_z component simulations using a natural distribution of Er^{3+} isotopes fit well with the observed hyperfine structure (HFS) in Er^{3+} spectra. $^{167}Er^{3+}$ isotope with a nuclear spin I=7/2 and 23% abundance resulted in an approximately symmetrical HFS pattern of 8 satellite lines with 3.7% amplitude of the central line and with hyperfine splitting $A_z=1288$ MHz, $A_y=518$ MHz and $A_x=120$ MHz for C_2 symmetry and $A_{\parallel}=1260$ MHz and $A_{\perp}=350$ MHz for C_{3i} . However, g_z component of a rhombic C_2 signal and g_{\parallel} component of a C_{3i} signal in the odd nuclear isotope $^{167}Er^{3+}$ were slightly shifted from that associated with even isotopes and found to be 12.28 and 12.20, respectively (figure 1(b)). This indicates that odd isotope $^{167}Er^{3+}$ experiences slightly different environmental effects caused by a different effective crystal field.

To examine this phenomenon and to elucidate how these hyperfine states affect spin electronic structure and relaxation dynamics, we synthesized an isotopically purified $^{167}{\rm Er}^{3+}$ doped ${\rm Y_2O_3}$ sample with 20 ppm doping and observed a spectrum with a high density of hyperfine transitions indicative of nuclear spin for $^{167}{\rm Er}^{3+}$. The lowest field components g_z and g_{\parallel} components are composed of eight lines, each as expected from I=7/2 (figure 2(a)). Importantly, the central line associated with transitions of even isotopes at g=12.20 was significantly reduced, testifying to the isotopic purity of the sample. The g_y component for C_2 state of $^{167}{\rm Er}^{3+}$, however, does not show expected eight-line pattern, but instead 16 major lines of different intensities were observed. This spectrum could not be deconvoluted to the set of octets if one would assume existence

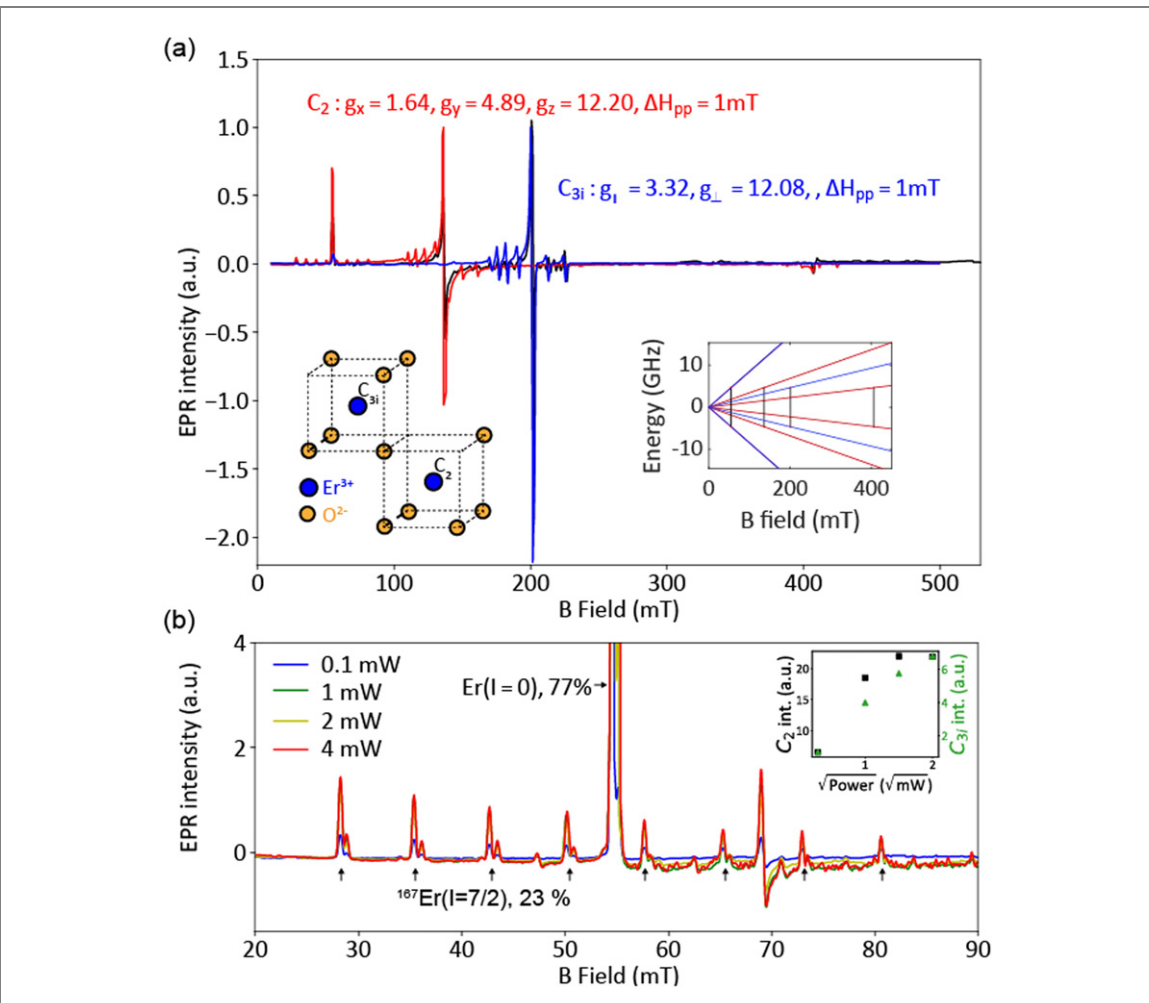


Figure 1. (a) CW-EPR spectroscopy provides spin Hamiltonian parameters for electron spin in the lowest doublet of ${}^4I_{15/2}$ under magnetic field. Inset left: ${\rm Er}^{3+}$ substitutes Y in the lower symmetry ${\rm C}_2$ site (bottom) and the higher symmetry ${\rm C}_{3i}$ site (top), Inset right: energy levels of g=12.20, 12.28, 3.32, 4.89 and 1.64 for ${\rm Er}^{3+}$ I=0 isotopes as function of B field (right), where X-band transitions are shown with black lines. CW-EPR on natural isotopic purity ${\rm Er}^{3+}:{\rm Y}_2{\rm O}_3$ shows transitions from ${\rm C}_2$ (red) and ${\rm C}_{3i}$ (blue) closely modelled by simulations. (b) The g=12.20 levels under close inspection reveal strong lines around 55 mT from I=0 isotopes of ${\rm Er}^{3+}$ along with two sets of 8 satellite lines corresponding to ${}^{167}{\rm Er}^{3+}$ from ${\rm C}_2$ g=12.28 and ${\rm C}_{3i}$ g=12.20. Inset: the g=12.20 lines from ${\rm C}_2$ and ${\rm C}_{3i}$ show different saturation with power.

of two nonidentical sites leading to two different hyperfine structures previously found in reference [21]. Our spectrum has very irregular line positions and intensities with separations that can be closely simulated with simple I = 7/2 nuclear hyperfine interactions A along with strong nuclear quadrupole interaction Q. Nuclear quadrupole interactions impose additional torque acting on 167 Er $^{3+}$ nuclei and affect quantization directions, thereby shifting energy levels and magnetic resonance transitions while also leading to forbidden transitions. Similarly, g_{\perp} component for C_{3i} state is now composed of more than 8 lines each, suggesting the presence of forbidden transitions. A similar observation was made for 167 Er $^{3+}$ in Y_2SiO_5 [8, 22] where forbidden transitions with intensity comparable to allowed transitions were described with a traceless nuclear quadrupole interaction (Q).

The spin Hamiltonian was fitted to the resonance fields for hyperfine transitions obtained from the experimental spectrum. We also assumed that g, A and Q tensors have coincident principal axes and can be simultaneously diagonalized as limited information about the orientation of the tensor can be derived from a powder spectrum alone for an anisotropic spin Hamiltonian. The low field transitions could be successfully fitted with g_z , A_z components of C_2 ($g_z=12.28$, $A_z=1280$ MHz) and g_{\parallel} of C_{3i} sites ($g_{\parallel}=12.20$, $A_{\parallel}=1268$ MHz), in both peak positions and their intensity (see supporting information S1). Intermediate field transitions were fitted to obtain g_y , A_y , Q [Q_x , Q_y , Q_z] terms of the C_2 site ($g_y=4.78$, $A_y=480$ MHz, Q=[-50, 10, 40] MHz) and g_{\perp} , A_{\perp} , Q [Q_{\parallel} , Q_{\perp}] terms of the C_{3i} site ($g_{\perp}=3.28$, $A_{\perp}=310$ MHz, Q=[12.5, -25] MHz). The C_2 g_x component at $g_x=1.64$ had broad transitions with small intensity which limited the number of hyperfine transitions to be resolved. Therefore, A_x was estimated from the difference in splitting of the lowest and highest field hyperfine transitions observed in the experimental spectrum ($g_x=1.64$, $A_x=212$ MHz). The simulated spectrum for C_2 site (red) and C_{3i} site (blue) generated using the fitted spin Hamiltonian shows

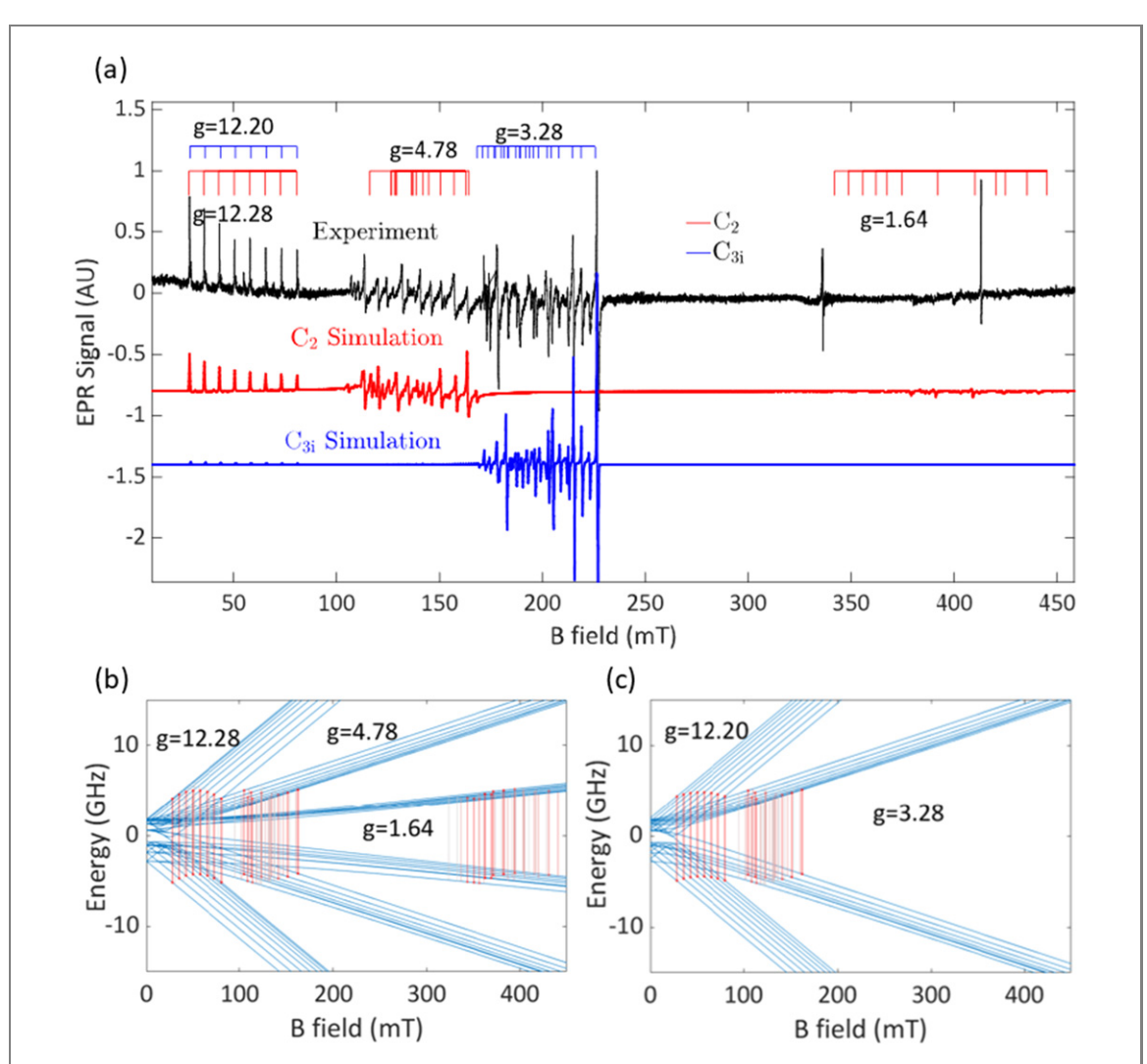


Figure 2. (a) 167 Er³⁺ X-band CW-EPR (black) compared with simulation for C₂ g = 12.28, g = 4.78, g = 1.64 and C_{3i} g = 12.20, 3.28 lines. Simulated spectra using Easyspin [20] show close agreement with the experimental spectrum. The predicted resonance fields for transitions are shown in dashed vertical dashes, grouped together for each g-factor. (b) & (c) 167 Er³⁺:Y₂O₃ simulated energy levels for (b) C₂ and (c) C_{3i} (blue) site as a function of field generated with Easyspin. Red lines show the high intensity X-band (9.3 GHz) transitions while the grey lines show lower intensity forbidden transitions.

Table 1. Spin Hamiltonian parameters for Er^{3+} (I = 0) in Y_2O_3 .

	C_2	C_{3i}
Electron Zeeman (g)	$g_x = 1.64, g_y = 4.89, g_z = 12.20$	$g_{\perp} = 3.32, g_{\parallel} = 12.08$

Table 2. Spin Hamiltonian parameters for $^{167}{\rm Er^{3+}}$ (I=7/2) in ${\rm Y_2O_3}$.

	C_2	C_{3i}
Electron Zeeman (g)	$g_x = 1.64, g_y = 4.78, g_z = 12.28$	$g_{\perp} = 3.28, g_{\parallel} = 12.20$
Hyperfine (A) (MHz)	$A_x = 212, A_y = 480, A_z = 1280$	$A_{\perp} = 310, A_{\parallel} = 1268$
Quadrupole (Q) (MHz)	$Q_x = 10, Q_y = 40, Q_z = -(Q_x + Q_y)$	$Q_{\perp} = 12.5, Q_{\parallel} = -2Q_{\perp}$

a close agreement to experimental spectrum in terms of peak position, shape as well as the relative intensity (figures 2(a) and (b)). Tables 1 and 2 summarize the principal values of g tensor for Er^{3+} (I=0) and g, A, Q for $^{167}Er^{3+}$ (I=7/2), respectively.

The predictions from an anisotropic 167 Er $^{3+}$ spin Hamiltonian fitted with the X-band EPR have been shown to exhibit disagreement with the low field EPR measurements in low symmetry hosts such as Y_2SiO_5 [21]. Therefore, to validate the fitted spin Hamiltonian at a lower field, we performed CW-EPR on the 167 Er $^{3+}$: Y_2O_3 sample with a C-band microwave (resonance frequency of 4.96 GHz) loop-gap cavity. The experimental spectra (figure 3) show close agreement with simulated spectrum from C_2 and C_{3i} sites and suggest a good estimate of

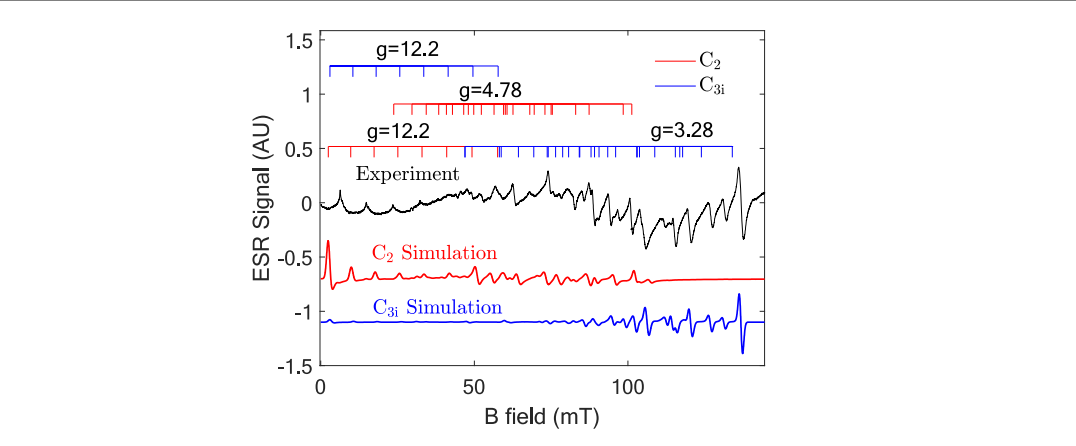


Figure 3. 167 Er $^{3+}$ 5 GHz CW-EPR spectrum (black) compared with spectra simulated from C_2 g = 12.20, g = 4.78 and C_{3i} g = 12.2, g = 3.28 lines. Simulated spectra using Easyspin [20] shows close agreement with the experimental spectrum. The predicted transition fields are shown in dashes, grouped together for each g factor.

EPR parameters. The fitted g values are also in close agreement with previous optical and EPR measurements [23–25].

We sent $\pi/2$ and π pulses and swept the magnetic field to obtain two pulse-field swept echo, (2P-FSE), $(\pi/2-\tau-\pi-\tau-\text{echo}, \tau=250 \text{ ns})$ spectrum of $^{167}\text{Er}^{3+}$ in X-band. Figure 4 shows EPR transition from hyperfine split levels which show similarities to the CW EPR spectrum of the same sample (supplement figure S2). The signal is temperature dependent, disappearing at 15 K, which is indicative of EPR signals of Er³⁺ ions. Four different regions of discrete multiline transitions are observed in addition to a broad underlined absorption that suggests existence of unresolved hyperfine structures of strongly interacting ¹⁶⁷Er³⁺ ions. The signal intensity ratio for C_{3i} : C_2 states in the 2P-FSE spectrum is higher compared to their intensity ratio in CW EPR, suggesting different spin dynamics of C3i and C2 states. Moreover, the 2P-FSE spectrum features are strongly dependent on the delay time τ between $\pi/2$ and π pulses, revealing individual dynamic features of C_2 , C_{3i} and strongly interacting ¹⁶⁷Er³⁺ sites. The strongly interacting sites show the fastest decay. Figure 4(a) shows the change of the 2P-FSE spectra with the change of the delay time au between two pulses. As au increases from 250 to 400 ns, the first signal to lose the intensity is the broad feature under the discrete transitions that we associate with strongly interacting ¹⁶⁷Er³⁺ sites. In the same time frame, discrete transitions become even more intense, possibly because of their diminished relaxation due to the decay of the strongly interacting species. At later times both C_2 and C_{3i} sites lose their intensity, and at $\tau = 1.5 \ \mu s$ only one pronounced transition remains, corresponding to the energetically highest m = +7/2 hyperfine state of C_{3i} .

While all low field spectral features for $^{167}\text{Er}^{3+}$ in rhombic crystalline environment C_2 vanish for the pulse delay of 1.5 μ s, figure 4(b) shows decay of the spectral features for high field g=1.64 C_2 component with increasing delay time τ . These features, although weak, persists for up to τ delay time of 3 μ s, suggesting their long coherence time. Temperature dependence of this signal is consistent with the temperature behavior of Er^{3+} signals at g=4.8 and 12.2 which also disappear at 15 K. The g=1.64 transition exhibited very slow stretched exponential echo decay with $T_2=24.4$ μ s measured at 4.3 K which was superimposed with slow nuclear modulation (figure 4(c)). The Fourier transform of electron spin envelope echo modulations ESEEM (obtained using 3P-ESEEM, $\pi/2-\tau-\pi/2-T-\pi/2-\tau$ – echo, with 16 step phase cycling) shown in figure 4(d) reveals two modulation frequencies, one stronger component of 0.45 MHz consistent with modulation of $^{167}\text{Er}^{3+}$ and one 0.80 MHz consistent with modulation of ^{89}Y suggesting that the interaction with $^{167}\text{Er}^{3+}$ ions from C_{3i} sites and to a lesser extent weakly coupled ^{89}Y 'matrix' nuclei contribute as a source of decoherence. However, due to the weak signal intensity, we were not able to measure spin lattice relaxation T_1 of the transition with g=1.64.

Transitions with higher g factors (g=12.2, 4.78, 3.28) exhibit stronger sensitivity to magnetic noise leading to the fast echo decay with a shorter T_2 time of approximately (0.5–0.9 μ s) (figure 4(e) for g=4.78 & table 3). The g=4.78 transition could be effectively dynamically decoupled from the sources of decoherence by applying a single XY16 [26] sequence, prolonging its T_2 for an order of magnitude to 3.9 μ s. Extending of coherence time obtained by applying dynamic decoupling sequences with multiple rotation axes such as XY16 demonstrates the presence of spectral diffusion as a source of fast spin decoherence. However, applying multiple sequences of XY16 only shortens spin coherence time T_2 due to pulse error. Only after the sign of the signal was inverted by applying a π pulse between two XY16 sequences, we obtained further enhancement of the spin coherence to 6.5 μ s. The signal obtained after dynamic decoupling reveals slow modulations reminiscent of

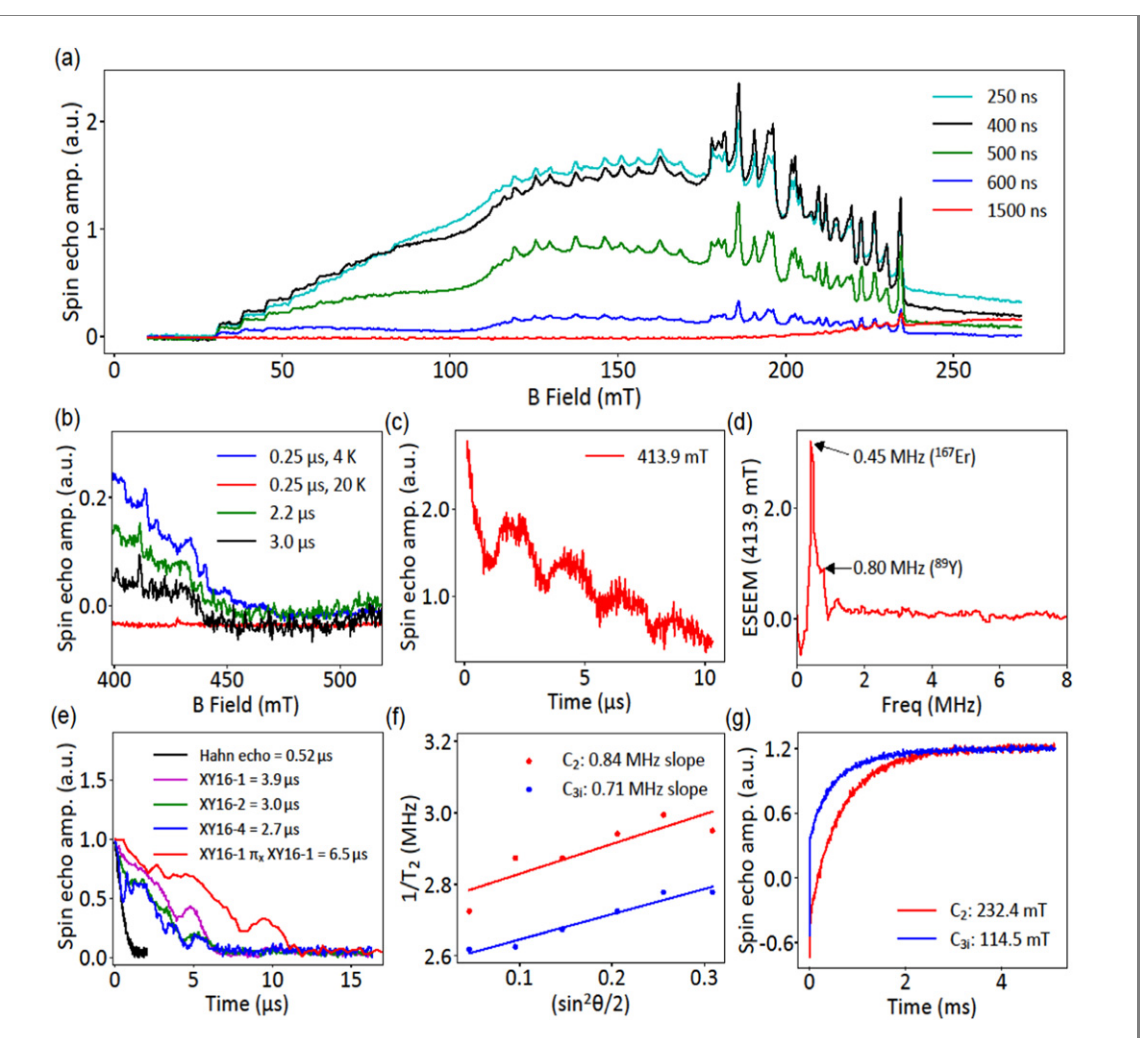


Figure 4. X-band pulsed EPR on $^{167}\text{Er}^{3+}:Y_2O_3$ at 4 K. (a) Echo detected field sweep shows EPR transition from hyperfine levels of C_2 g=12.28, 4.78 and C_{3i} g=12.20, 3.28 along with a short lived broad unresolved signal due to $^{167}\text{Er}^{3+}$ interaction. At pulse separation of 1.5 μ s only signal from C_{3i} $m_S=+7/2$ remains. (b) C_2 g=1.64 component shows slow decay and persists up to 3 μ s at 4 K while decays completely at 20 K. (c) The echo decay of g=1.64 signal shows stretched exponential decay corresponding to coherence time of 24.4 μ s superimposed to electron spin echo envelope modulation (ESEEM). (d) The fast Fourier transform of three pulse ESEEM (frequency domain) for g=1.64 component reveals Larmor frequencies for $^{167}\text{Er}^{3+}$ and $^{89}\text{Y}^{3+}$ nuclei at 413.9 mT. (e) The integrated area echo decay for C_2 g=4.89 transition shows a coherence time of 0.5 μ s with further improvement to 6.5 μ s after applying XY-16- π -XY-16 DD sequence. (f) Instantaneous diffusion measurement on C_2 g=4.78 and C_{3i} g=3.28 with slope 0.84 and 0.71 MHz respectively. (g) T_1 measurement on C_2 g=4.78 and C_{3i} g=3.28 transition with inversion recovery sequence.

those obtained in 3P ESEEM measurements of g = 1.64 transition, suggesting that the same ions participate in relaxation of spins with g = 4.78.

Instantaneous diffusion [27] arising from the dipole interaction of resonant $^{167}\text{Er}^{3+}$ spins during inversion pulses is another mechanism of spin decoherence. We investigated instantaneous diffusion by applying the Hahn echo ($\pi/2 - \tau - \Theta - \tau$ – echo) sequence with various spin-flip angles. Figure 4(f) shows the dependence of $1/T_2$ of C_2 g=4.89 measured as a function of different spin-flip probability ($\sin^2\Theta/2$, where Θ is spin-flip angle). We obtain a linear dependence of the $1/T_2$ on the average spin flip probability with the slope of 0.8 MHz, suggesting an effective concentration of resonant spins with density 1.38×10^{17} spin/cm³ (equivalent dopant density of \sim 5 ppm) with g=4.78 contributing to instantaneous diffusion. The instantaneous diffusion determined for the spins in C_{3i} symmetry (figure 4(f)) shows very similar dependence of $1/T_2$ on the spin flip probability $\sin^2\Theta/2$ (slope of 0.7 MHz) corresponding to an estimated density of 2.53×10^{17} spins/cm³ with g=3.28.

The electron spins in highly symmetric C_{3i} sites also experience spectral diffusion from spin flips of neighboring spins that could be mitigated through XY16 dynamic decoupling pulse sequences. Applying the multiple XY16 sequences separated by a sign inversion π pulse, extends coherence time T_2 of C_{3i} states up to 6 μ s measured at 4.2 K. However, decoupling schemes do not extend the coherence time up to the T_1 limits given by spin-lattice relaxation. Spin lattice relaxation times were determined through three pulse inversion recovery sequence ($\pi - T - \pi/2 - \tau - \pi - \tau$ – echo with 4 step phase cycling) and were found to be biexponential

Table 3. Spin relaxation time and coherence time for $^{167}\mathrm{Er^{3+}}$ at 4 Kelvin.

g-factor	Group	Field	T ₁ long comp	T ₁ short comp	Ratio long:short	T_2
		314 G	4.8 ms	0.1 ms	5:3	0.9 μs
12.2 C ₂ /C	C_2/C_{3i}	386 G	3.2 ms	0.8 ms	4:3	$0.8~\mu s$
		586 G	2.8 ms	0.9 ms	1.4:3	$0.5~\mu \mathrm{s}$
		1125 G	700 μs	13 μs	4:1	$0.4~\mu s$
4.8	C_2	1189 G	$640~\mu s$	$12 \mu s$	4:1	$0.4~\mu s$
		1372 G	$620~\mu s$	$47~\mu s$	5:1	$0.4~\mu \mathrm{s}$
3.3 C _{3i}		1858 G	580 μs	$4 \mu s$		$0.4~\mu s$
	C_{3i}	1958 G	580 μs	$4 \mu \mathrm{s}$		$0.4~\mu s$
		2342 G	$580 \mu s$	$4~\mu s$		$0.4~\mu \mathrm{s}$
1.6	C ₂	4139 G	Too weak to measure			24.4 μs
Broad signs	al no hyperfine	1030 G	0.35 ms	$8.6~\mu \mathrm{s}$	7:2	0.3 μs

Table 4. Spin relaxation time and coherence time for Er³⁺ natural isotopic abundance at 4 Kelvin.

g group	Field	T_1	T_2	Group
12.2 4.9 3.3 1.6	534 G 1389 G 2045 G 4121 G	1.7 μs 16 μs 7.6 μs 16 μs	$<$ 200 ns 1.5 μ s 1.1 μ s 0.6 μ s	$C_2/C_{3i} \\ C_2 \\ C_{3i} \\ C_2$

with larger fraction of the slow component (table 3). Determined slow component of T_1 is long for $^{167}{\rm Er}^{3+}$ in C_{3i} states, reaching 0.6 ms at 4.2 K. As T_1 spin-lattice relaxation bounds coherence time, long T_1 times suggests orders of magnitude improvement of electron spin coherence times by eliminating spectral and instantaneous diffusion. The spin lattice relaxation times of C_2 states are even longer ranging from 0.7 ms for g=4.78, to 5 ms for g=12.20 at 4.2 K. The T_1 times for $^{167}{\rm Er}^{3+}$ are significantly longer than that of natural isotopic abundance ${\rm Er}^{3+}$ sample with three orders of magnitude longer T_1 for C_2 g=12.2, an order of magnitude for C_2 g=4.8 and for C_{3i} g=3.3 (table 4). These results suggest that isotope inhomogeneity in natural isotope promotes spin-lattice decays.

3. Conclusion

We have comprehensively characterized the spin Hamiltonian of ground state 167 Er $^{3+}$ in both C_2 and C_{3i} sites of Y_2O_3 using X-band EPR. The spin Hamiltonian exhibited an anisotropic g, A matrix with a strong nuclear quadrupole interaction Q leading to forbidden EPR transitions and showed good agreement with the 5 GHz CW-EPR spectra. The measured strong anisotropic hyperfine interaction of 167 Er $^{3+}$ in both C_2 and C_{3i} sites of Y_2O_3 suggests the presence of zero first-order Zeeman (ZEFOZ) transitions at low fields with possibly long spin coherence times [9,28]. The spin dynamics of 167 Er $^{3+}$ studied using X-band pulsed EPR show a long coherence time reaching $24.4~\mu s$ for g=1.64 transition at 4 K. The spin coherence time was found to be limited by spectral diffusion with and instantaneous diffusion for both C_2 and C_{3i} sites. With lower doping concentration the spin coherence time could be further improved at 4 K. Addressing low field ZEFOZ transitions and utilizing pulsed sequences aimed at decoupling dipolar interaction and spectral diffusion [29] could be future steps in maximizing the coherence of this system for enabling quantum technologies.

Acknowledgement

We acknowledge Oleg Poluektov and Jens Niklas for D-Band EPR measurements.

Author contributions

The manuscript was written through contributions of all authors. JY and HZ prepared the samples; TR and LS performed X-band EPR spectroscopy. SG & TZ performed 5 GHz EPR spectroscopy. TR, LS, SG and TZ analyzed and simulated EPR spectra. All authors have given approval to the final version of the manuscript.

Funding sources

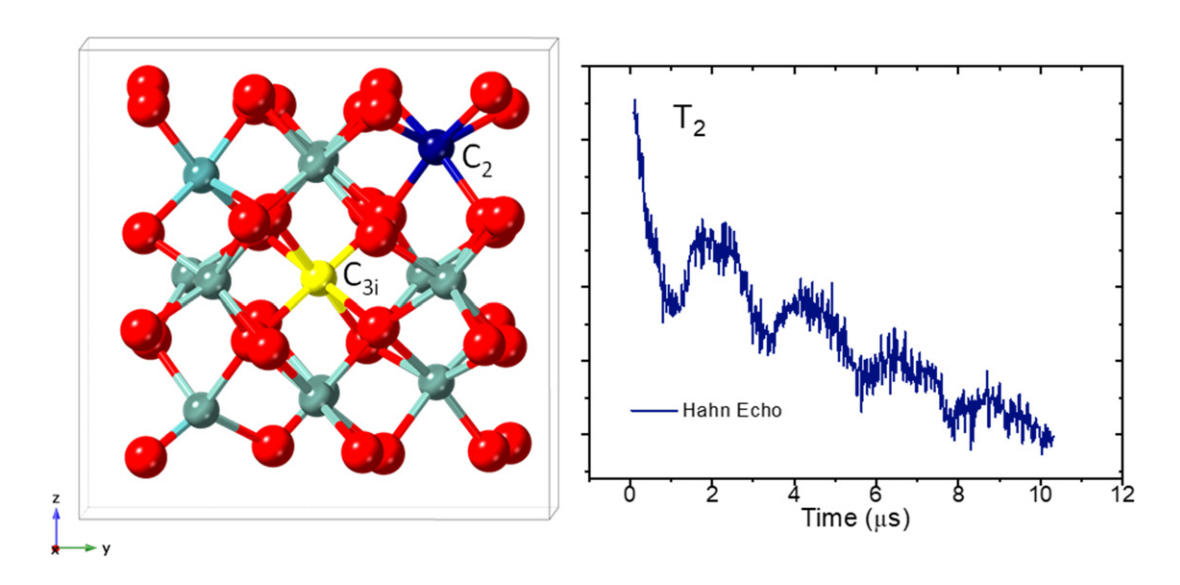
This work was supported by the US Department of Energy, Office of Science, Basic Energy Sciences, Materials Science and Engineering Division. S Gupta and T Zhong acknowledge the support from Department of Defense, Army Research Office Grant No. W911NF2010296, and National Science Foundation (NSF) Faculty Early Career Development Program (CAREER) Grant (No. 1944715). Work performed at the Center for Nanoscale Materials, a US Department of Energy Office of Science User Facility, was supported by the US DOE, Office of Basic Energy Sciences, under Contract No. DE-AC02-06CH11357.

Notes

The authors declare no competing financial interests.

Abbreviations

CW-EPR, continuous-wave electron paramagnetic resonance; ZEFOZ, zero-first-order Zeeman; ESEEM, electron spin echo envelope modulation.



Data availability statement

The data that support the findings of this study are available upon reasonable request from the authors.

ORCID iDs

Lei Sun https://orcid.org/0000-0001-8467-6750
Tian Zhong https://orcid.org/0000-0003-3884-7453

References

- [1] Thiel C W, Böttger T and Cone R L 2010 Rare-earth-doped materials for applications in quantum information storage and signal processing *J. Lumin.* 131 353
- [2] Zhong M, Hedges M P, Ahlefeldt R L, Bartholomew J G, Beavan S E, Wittig S M, Longdell J J and Sellars M J 2015 Optically addressable nuclear spins in a solid with a six-hour coherence time *Nature* 517 177
- [3] Rančić M, Hedges M P, Ahlefeldt R L and Sellars M J 2018 Coherence time of over a second in a telecom-compatible quantum memory storage material Nat. Phys. 14 50
- [4] Lauritzen B, Minář J, de Riedmatten H, Afzelius M and Gisin N 2011 Approaches for a quantum memory at telecommunication wavelengths *Phys. Rev.* A 83 012318
- [5] Kimble H J 2008 The quantum internet *Nature* 453 1023
- [6] Kurizki G, Bertet P, Kubo Y, Mølmer K, Petrosyan D, Rabl P and Schmiedmayer J 2015 Quantum technologies with hybrid systems Proc. Natl Acad. Sci. USA 112 3866
- [7] Degen C L, Reinhard F and Cappellaro P 2017 Quantum sensing Rev. Mod. Phys. 89 035002

- [8] Guillot-Noël O, Goldner P, Du Y L, Baldit E, Monnier P and Bencheikh K 2006 Hyperfine interaction of Er³⁺ ions in Y₂SiO₅: an electron paramagnetic resonance spectroscopy study *Phys. Rev.* B **74** 214409
- [9] Rakonjac J V, Chen Y H, Horvath S P and Longdell J J 2020 Long spin coherence times in the ground state and in an optically excited state of Er³⁺167:Y₂SiO₅ at zero magnetic field *Phys. Rev.* B 101 184430
- [10] Fukumori R, Huang Y, Yang J, Zhang H and Zhong T 2020 Subkilohertz optical homogeneous linewidth and dephasing mechanisms in Er³⁺:Y₂O₃ ceramics *Phys. Rev.* B 101 214202
- [11] Zhang H et al 2017 Transparent Er^{3+} -doped Y_2O_3 ceramics with long optical coherence lifetime ACS Omega 2 3739
- [12] Zhong T and Goldner P 2019 Emerging rare-earth doped material platforms for quantum nanophotonics Nanophotonics 8 185
- [13] Scarafagio M et al 2019 Ultrathin Eu- and Er-doped Y₂O₃ films with optimized optical properties for quantum technologies J. Phys. Chem. C 123 13354
- [14] Singh M K, Prakash A, Wolfowicz G, Wen J, Huang Y, Rajh T, Awschalom D D, Zhong T and Guha S 2020 Epitaxial Er-doped Y₂O₃ on silicon for quantum coherent devices *APL Mater.* 8 031111
- [15] Bartholomew J G, de Oliveira Lima K d O, Ferrier A and Goldner P 2017 Optical line width broadening mechanisms at the 10 kHz level in Eu³⁺:Y₂O₃ nanoparticles *Nano Lett.* 17 778
- [16] Serrano D, Deshmukh C, Liu S, Tallaire A, Ferrier A, de Riedmatten H and Goldner P 2019 Coherent optical and spin spectroscopy of nanoscale Pr^{3+} : Y_2O_3 *Phys. Rev.* B 100 144304
- [17] Abragam A and Bleaney B 1970 EPR of Transition Metal Ions (Oxford: Clarendon)
- [18] Skvortsov A, Savchenko D, Potucek Z, Jastrabik L, Trepakov V and Dejneka A 2014 Optical and EPR characterization of Er³⁺ centers in SrTiO₃ single crystals Phys. Status Solidi B 251 2270
- [19] Antuzevics A 2020 EPR characterization of erbium in glasses and glass ceramics Low Temp. Phys. 46 1149
- [20] Stoll S and Schweiger 2006 EasySpin, a comprehensive software package for spectral simulation and analysis in EPR J. Magn. Reson. 178 42
- [21] Vincent J, Guillot-Noël O, Binet L, Aschehoug P, Le Du Y L, Beaudoux F and Goldner P 2008 Electron paramagnetic resonance and optical spectroscopy of Er-doped β-Ga₂O₃ *J. Appl. Phys.* **104** 033519
- [22] Chen Y H, Fernandez-Gonzalvo X, Horvath S P, Rakonjac J V and Longdell J J 2018 Hyperfine interactions of Er³⁺ ions in Y₂SiO₅: electron paramagnetic resonance in a tunable microwave cavity *Phys. Rev.* B **97** 024419
- [23] Harris T L 2001 Erbium-based optical coherent transient corelator for the 1.5-micron communication bands PHD Thesis Montana State University
- [24] Schäfer G and Scheller S 1966 Paramagnetisehe resonanz yon Er3+ in Y2O3 Phys. Condens. Mater. 5 58
- [25] Reinemer G D 2003 Optical characterization of perturbed sites and C_{3i} sites in rare earth doped oxide crystals PhD Thesis Montana State University
- [26] Gullion T, Baker D B and Conradi M S 1990 New, compensated Carr-Purcell sequences J. Magn. Reson. (1969) 89 479
- [27] Agnello S, Boscaino R, Cannas M and Gelardi F M 2001 Instantaneous diffusion effect on spin-echo decay: experimental investigation by spectral selective excitation Phys. Rev. B 64 174423
- [28] Ortu A, Tiranov A, Welinski S, Fröwis F, Gisin N, Ferrier A, Goldner P and Afzelius M 2018 Simultaneous coherence enhancement of optical and microwave transitions in solid-state electronic spins Nat. Mater. 17 671
- [29] Zhou H et al 2020 Quantum Metrology with strongly interacting spin systems Phys. Rev. X 10 031003